Advances in Engineering Software 144 (2020) 102791

Contents lists available at ScienceDirect

Advances in Engineering Software

journal homepage: www.elsevier.com/locate/advengsoft

Research paper

Overlapping finite element meshes in AMORE

Junbin Huang, Klaus-Jürgen Bathe*

Department of Mechanical Engineering, Massachusetts Institute of Technology, Cambridge, MA 02139, USA

ARTICLE INFO

Keywords:
Finite elements
Overlapping elements
CAD
Meshing
AMORE paradigm
Solvability and convergence

ABSTRACT

The AMORE scheme of "automatic meshing with overlapping and regular elements" has been recently proposed, in which the concept of overlapping finite elements plays a central role. In earlier work we focused on the overlapping of individual elements. In this paper, we present a technique to overlap finite element meshes so that elements from different meshes can overlap in any geometric form. Meshes for different parts of the analysis domain can be independently spanned, which is an effective way to adapt meshes to various geometric features and solution gradients. Hence, the meshing effort is much reduced and high solution accuracy is achieved. We formulate the new scheme, analyze its solvability and convergence, and propose an implementation. The solutions of some engineering problems are given to illustrate the use and performance of the new scheme.

1. Introduction

Great advances have been achieved for finite element analyses during the past decades. However, in engineering practice, much human effort is still required for initiating a finite element analysis, specifically for meshing the analysis domain [1].

Reducing the meshing effort has long been an active research area. In computational fluid mechanics, Chimera grids, also called composite overlapping grids or overset grids, have been used with finite difference methods and finite volume methods [2–4]. These enable convenient local refinements near obstacles and boundaries, hence can give good predictions for local solutions. Similar procedures in finite element analysis have not been as successful due to the requirement of compatibility of finite element approximations. For finite element methods, several published methods can be used to simplify the meshing of complex analysis domains, specifically the domain decomposition method [5], the generalized finite element method [6–8], Nitsche's method [9,10], and the fictitious domain method [11,12]. The domain decomposition method uses the divide-and-conquer concept to solve a large system of equations by iteratively solving for each small subdomain and exchanging information with neighboring subdomains. It is not an interpolation scheme that is being pursued. In the generalized finite element method, a regular mesh that covers a domain larger than of interest is used for approximation, but the integration is only performed over the physical domain of interest by using an adaptive integration scheme, see also [13] for a similar idea. Nitsche's scheme is used for several non-matching meshes that overlap, but the overlapped regions are deleted and the interface conditions are imposed using a penalty term. The fictitious domain method considers an extended variational problem on a larger domain containing the original analysis domain, and the boundary conditions are imposed weakly by using Lagrange multipliers. These methods address the effort of meshing, however with the cost of losing several advantages of traditional finite element methods, and the methods have not been widely accepted in the engineering community for the finite element analyses of solids.

We propose here a method of overlapping finite element meshes in which a global compatible interpolation is obtained, and the meshing process can be highly automated with a reasonable computational expense.

To significantly reduce the effort in meshing, the AMORE (automatic meshing with overlapping and regular elements) paradigm of finite element analysis has been recently proposed [14–19], which does not only reduce the meshing effort, but also accurately captures the boundary stresses. The key idea of the procedure is to use undistorted traditional elements for the interior of the domain, and novel overlapping elements near the boundaries. To simplify the discretization of complex domains, severe distortions are allowed for the overlapping elements because they are distortion-insensitive. In the procedure conforming elements are used throughout, and spheres/disks, triangular and quadrilateral elements have been considered as overlapping elements. In the most efficient scheme, to formulate the overlapping elements, the attractive aspects from traditional elements and the method of finite spheres are used.

Hence the basic premise in AMORE is that, on a geometry, elements and meshes are spanned that can overlap in order to reduce the meshing effort [14]. Since CAD functions are not used, the geometry

* Corresponding author.
E-mail address: kjb@mit.edu (K.-J. Bathe).

https://doi.org/10.1016/j.advengsoft.2020.102791
Received 23 January 2020; Accepted 21 February 2020
Available online 24 April 2020

can be given by any CAD program or by a computerized scan. While we focused first on individual overlapping elements and their coupling to regular elements, we propose here a specific scheme in which complete meshes with their elements can overlap freely.

In this scheme, the meshing of the complete domain is accomplished by the steps of AMORE in which first a regular grid is spanned over the complete geometry, cells outside or cutting the boundary are removed, the remaining cells are turned into undistorted regular finite elements, and the empty space is filled with overlapping elements. The novel aspect we present in this paper is that the overlapping elements to fill the empty space are now complete meshes. For each mesh, a local compatible interpolation is given using any existing interpolation technique. To establish a global compatible field, weight functions are formulated satisfying the partition of unity property. Using undistorted traditional elements in the interior domain and higher-order elements for the boundary domains that overlap can be efficient also to obtain accurate local solutions of stress concentrations.

In the following, we first present the formulation of the method of overlapping finite element meshes. We then discuss the solvability and convergence of the procedure and briefly focus on an efficient implementation of the scheme. Next we illustrate the performance of the proposed method in the solution of simple problems to obtain insight, and then use AMORE in the solution of some more complex problems to illustrate the use of overlapping meshes. Finally we give our concluding remarks pointing out the potential of the method for general finite element analysis.

2. The interpolation for overlapping finite element meshes

The analysis domain is first divided into several subdomains, each of which is then meshed independently. If the domain decomposition is reasonable, each subdomain is of regular shape and can be given a regular conforming mesh. Any interpolation technique may be chosen for a mesh as long as the interpolation is compatible. Good candidates include the isoparametric interpolations [1], the finite elements enriched by interpolation covers [21], and the overlapping finite elements [14–20]. For simplicity, we use in this paper the traditional isoparametric interpolations.

The key idea of the method of overlapping finite element meshes is to couple these (local) fields (interpolated independently over each subdomain) to form a global interpolation with desired compatibility and accuracy. To this aim, continuous weight functions are automatically computed for each mesh. The weighted average of local fields serves as the global interpolation for the solution.

2.1. Domain decomposition

Let us consider static problems in two-dimensional linear elasticity. The analysis domain Ω is decomposed into several subdomains Ω_i ($i = 1, \ldots, m$). The boundary of the analysis domain is denoted by $\partial\Omega$. Each subdomain Ω_i has its own boundary $\partial\Omega_i$. We further define $\Gamma_i = \partial\Omega_i \cap \partial\Omega$ and $\Gamma_i^* = \partial\Omega_i \cap \Omega$, where Γ_i represents the exterior boundary of Ω_i and Γ_i^* represents the interior boundary. For these subdomains to form a decomposition of Ω, i.e. $\Omega = \cup_{i=1}^m \Omega_i$, the subdomains have to overlap rather than just touch each other. In other words, each overlapped region should not degenerate to a curve. An example of a proper domain decomposition is given in Fig. 1.

In finite element analysis, non-matching meshes are occasionally used to simplify meshing. Although non-matching meshes are not permitted in the proposed method (because there is no overlapped region), they may be interpreted as a limit case, see Sections 2.5 and 3.2.

On each subdomain Ω_i, a conforming mesh $\mathcal{T}_i$ is spanned as in traditional finite element analysis. Note that each subdomain is discretized independently. Each mesh has its own nodes and degrees of freedom (dofs) even though two nodes from different meshes may have the same coordinates.

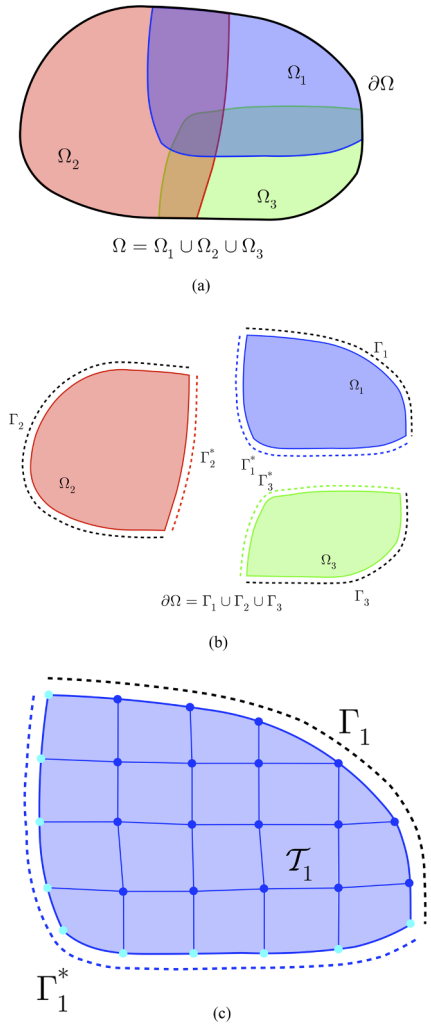

Fig. 1. An example of a proper domain decomposition, $m = 3$. (a) Subdomains, (b) Boundaries of subdomains, (c) Mesh on a subdomain (the function P_1 is assigned 0 at cyan nodes and 1 at blue nodes).

The meshes of the subdomains form a mesh overlay for the complete analysis domain. To construct a global compatible interpolation, the structure of the mesh overlay needs to be computed and stored effectively. Fortunately, there are existing algorithms from computational geometry that can be modified for our purpose [22,23].

2.2. Weight functions

Each local interpolation contributes to the global interpolation by a weight function. These functions form a partition of unity on the whole analysis domain. Formally, the weight function $w_i(\mathbf{x})$ ($i = 1, \ldots m$) are defined to satisfy the following conditions, where $\mathbf{x} = (x, y)$.

1) The weight functions are continuous, non-negative functions over the analysis domain;
2) Each weight function $w_i(\mathbf{x})$ vanishes outside Ω_i;
3) The condition $\sum_{i=1}^m w_i(\mathbf{x}) = 1$ holds on Ω.

These requirements ensure that, if each local interpolation is compatible and contains an arbitrary linear field, the global interpolation does so as well. Hence the constant stress patch tests are satisfied.

Let $P_i(\mathbf{x}) = \sum_j h_j^i(\mathbf{x}) p_j^i$ be a function on the subdomain Ω_i, where $h_j^i(\mathbf{x})$ is the shape function used in low-order finite elements, and p_j^i is the weight at the jth node in mesh $\mathcal{T}_i$. For a mixed mesh with both

quadrilaterals and triangles, both bilinear shape functions (for quadrilaterals) and linear shape functions (for triangles) are used. To satisfy the second requirement, $P_i(\mathbf{x})$ must vanish on the closure of Γ_i^*. Thus, we assign $p_j^i = 0$ if the corresponding node is on the closure of Γ_i^*. As shown in Fig. 1(c), other nodes in the mesh are assigned the weight 1. Now the first requirement is also fulfilled because $P_i(\mathbf{x})$ can be continuously extended to the whole analysis domain. To satisfy the partition of unity property, the weight functions are defined as

$$w_i(\mathbf{x}) = \frac{\alpha_i P_i(\mathbf{x})}{\sum_j \alpha_j P_j(\mathbf{x})} \tag{1}$$

where we use $\alpha_1 = 1$ and $\alpha_2 = \ldots = \alpha_m = 9$ because in our scheme the first mesh is usually a regular 4-node finite element mesh for the interior subdomain and the other meshes have higher-order interpolations to resolve the boundary stress concentrations and the boundary curvature. The choice of α reflects that if a lower-order mesh is coupling with a higher-order mesh, the scheme should put more weight on the higher-order interpolation.

In a reasonable mesh, $P_i(\mathbf{x})$ is strictly positive for all $\mathbf{x}$ in Ω_i. Since $\Omega = \cup_{i=1}^m \Omega_i$, $\Sigma \alpha_j P_j(\mathbf{x}) > 0$ holds everywhere inside the analysis domain. Therefore, Eq. (1) is well defined and conditions 1) to 3) are satisfied. In Section 2.5, we discuss an example of an invalid mesh, for which the denominator in Eq. (1) may vanish. Such case should be avoided and the procedure needs to first check the validity of overlapping meshes.

We see from Eq. (1) that the weight functions are rational functions. Numerically integrating terms involving rational functions can be computationally expensive. Hence, in the actual implementation, we interpolate the weight functions by linear functions without violating any requirement, see Section 2.6.

2.3. The interpolation and stiffness matrix

Assume local interpolations of the displacement have been established upon each mesh:

$$\mathbf{u}_i(\mathbf{x}) = \mathbf{H}_i(\mathbf{x})\mathbf{q}_i \tag{2}$$

where $\mathbf{u}_i(\mathbf{x})$ is the interpolated displacement vector on the ith mesh, $\mathbf{H}_i(\mathbf{x})$ is the shape function matrix for the ith mesh, and $\mathbf{q}_i$ is the corresponding vector of degrees of freedom. As mentioned above, any interpolation technique can be used for local interpolations as long as the resulting field is compatible on the corresponding subdomain. In this paper, we use traditional isoparametric interpolations.

The global interpolation is the weighted average of the local interpolations using the weight functions defined in the preceding section:

$$\mathbf{u}(\mathbf{x}) = \sum_{i=1}^m w_i(\mathbf{x})\mathbf{u}_i(\mathbf{x}) = \sum_{i=1}^m w_i(\mathbf{x})\mathbf{H}_i(\mathbf{x})\mathbf{q}_i \tag{3}$$

The strain interpolation can be directly obtained from the displacements:

$$\boldsymbol{\varepsilon}(\mathbf{x}) = \sum_{i=1}^m \mathbf{B}_i(\mathbf{x})\mathbf{q}_i = [\mathbf{B}_1 \ \ldots \ \mathbf{B}_m]\begin{Bmatrix}\mathbf{q}_1\\ \vdots \\ \mathbf{q}_m\end{Bmatrix} \tag{4}$$

where

$$\mathbf{B}_i = \begin{bmatrix}\frac{\partial}{\partial x} & 0\\ 0 & \frac{\partial}{\partial y}\\ \frac{\partial}{\partial y} & \frac{\partial}{\partial x}\end{bmatrix}[w_i(\mathbf{x})\mathbf{H}_i(\mathbf{x})] \tag{5}$$

The stiffness matrix is given by

$$\mathbf{K} = \int_\Omega [\mathbf{B}_1 \ \ldots \ \mathbf{B}_m]^\top \mathbf{C}[\mathbf{B}_1 \ \ldots \ \mathbf{B}_m]\mathrm{d}\Omega \tag{6}$$

where $\mathbf{C}$ is the elastic stress-strain matrix, and we can also define

$$\mathbf{K}_{ij} = \int_\Omega \mathbf{B}_i^\top \mathbf{C}\mathbf{B}_j \mathrm{d}\Omega = \int_{\Omega_i \cap \Omega_j} \mathbf{B}_i^\top \mathbf{C}\mathbf{B}_j \mathrm{d}\Omega \tag{7}$$

The last equality is due to the fact that $\mathbf{B}_i$ vanishes outside Ω_i.

Eq. (7) shows that we need to integrate a piecewise continuous function over overlapped regions. The arbitrariness of the mesh overlay makes the numerical integration more difficult than in conventional finite element analysis. For those elements that do not overlap with others, the required integrations are evaluated as usual. To integrate the element contributions of the coupling regions, we first establish the geometric structure of the overlapping and divide the overlapped regions into polygons. Then each polygon is triangulated so that numerical integration schemes for triangular domains can be used [24,25], see Section 2.6.

2.4. Boundary conditions

We consider displacement boundary conditions and force boundary conditions. Let S_u be the part of the boundary on which displacements are prescribed, with $\mathbf{u} = \mathbf{u}_0$. Then for each subdomain for which $\Gamma_i \cap S_u \neq \emptyset$, $\mathbf{u}_i = \mathbf{u}_0$ needs be satisfied on the constrained boundary.

To impose the force boundary conditions we proceed as in general finite element analysis.

$$\begin{bmatrix}\delta\mathbf{q}_1\\ \vdots \\ \delta\mathbf{q}_m\end{bmatrix}^\top \mathbf{F} = \int_\Omega \delta\mathbf{u}\cdot\mathbf{b}\mathrm{d}\Omega + \int_{S_f} \delta\mathbf{u}\cdot\mathbf{f}\mathrm{d}S + \sum_c \delta\mathbf{u}(\mathbf{x}_c)\cdot\mathbf{P}_c \tag{8}$$

where δ is the variational symbol, $\mathbf{b}$ is the vector of external body force, S_f is the boundary on which the external boundary force $\mathbf{f}$ is imposed, and $\mathbf{P}_c$ is a concentrated external force acting at the point $\mathbf{x}_c$. Note that an external force acting on an overlapped region contributes to multiple meshes, while in traditional finite element analysis, all forces are imposed onto a single mesh.

2.5. Solvability and convergence

In this section, we analyze the condition for the proposed scheme to be solvable, using direct sparse solvers for symmetric positive definite systems, and we study the convergence rate of the scheme.

For static problems in linear elasticity, provided that the material parameters and boundary constraints are reasonable, the bilinear forms of the continuous problems are bounded and coercive. Therefore, the solution always exists and is unique. However, the finite element discretized equations may not be solvable because the formulation may be unstable [1,26,27]. In order to have a unique solution (after imposing appropriate displacement boundary conditions), any assignment of dofs must represent a unique displacement field. Equivalently, in order to obtain a zero field, all dofs must be zero. Therefore, we have the following necessary and sufficient condition for solvability.

Condition I (Necessary and Sufficient):

The equation

$$\mathbf{0} \equiv \sum_{i=1}^m w_i \mathbf{H}_i \mathbf{q}_i \tag{9}$$

has only the trivial solution with all $\mathbf{q}_i = 0$, i.e. only a zero assignment of the dofs can result into a zero displacement field. Here we assume that w_i is well-defined and further interpolated by a linear function over each triangle (see Section 2.6 for some details of the triangulation).

Although Condition I is all we need to satisfy, we cannot directly see whether it actually holds.

Consider the mesh in Fig. 2. Since we need to have $w_i > 0$ everywhere in Ω_i as mentioned in Section 2.2, we see that the mesh in Fig. 2 is invalid. All four nodes of element e are located on the interior boundary of Ω_i, hence P_i vanishes on element e, and so does the weight function w_i. As a result, the dofs at nodes 2 and 3 have no contribution

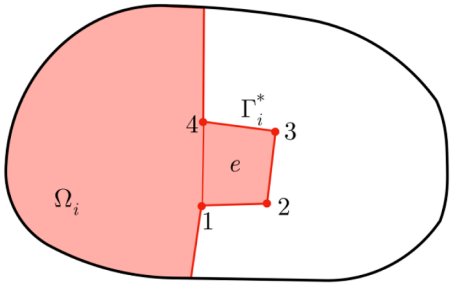

Fig. 2. An invalid mesh.

to the local field since derivatives of the elemental interpolation vanish on element e (see Eq. (3)). Therefore, Eq. (9) has a non-trivial solution, and the interpolation is unsolvable. It can be easily checked by a computer procedure whether this situation is present, and it will in general only be present if the mesh is very coarse. Hence we have the following necessary condition for the overlapping meshes to be solvable.

Condition II (Necessary):

For each i, $w_i > 0$ holds everywhere in Ω_i before the weight functions are further interpolated by linear functions.

Let us next assume Eq. (9) has a non-trivial solution, then there exists some j such that for a scalar field solution over the domain Ω_j with $u_j = \mathbf{H}_j\mathbf{q}_j \neq 0$, Eq. (9) can be rewritten as

$$w_j\mathbf{H}_j\mathbf{q}_j = -\sum_{i\neq j} w_i\mathbf{H}_i\mathbf{q}_i \tag{10}$$

which means that any displacement of one mesh (with its weight) must not be contained in any interpolation of another mesh, or union of the other meshes. This could be computationally checked in various ways.

In the implementation, Condition II can be easily checked by identifying whether in an element the corresponding weight function vanishes. To also satisfy Condition I, we can simply prevent the nodes in different meshes from having the same coordinates except for some boundary nodes. Of course, to improve the conditioning of the system, we can design a meshing procedure in which nodes from different meshes do not even have close coordinates.

Having established solvability, we can now give an error bound.

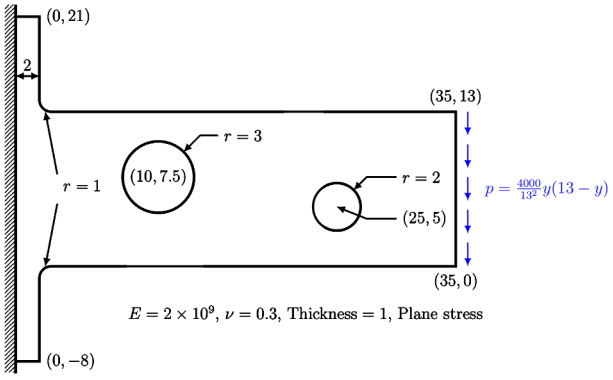

(a) Problem description

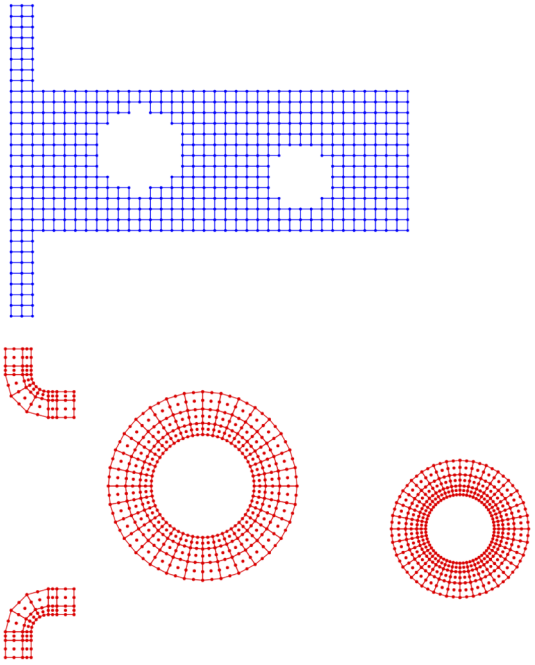

(b) The individual meshes used (not to scale)

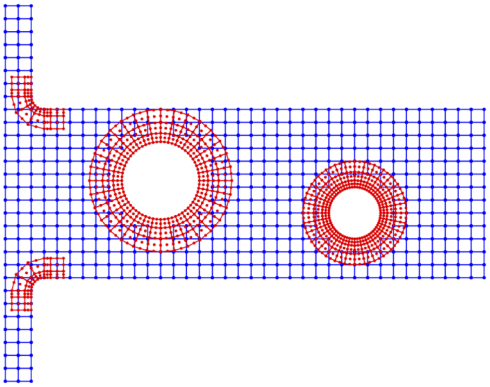

(c) Assembled meshes

Fig. 3. A plane stress plate problem and the overlapping meshes. (a) Problem description, (b) The individual meshes used (not to scale), (c) Assembled meshes.

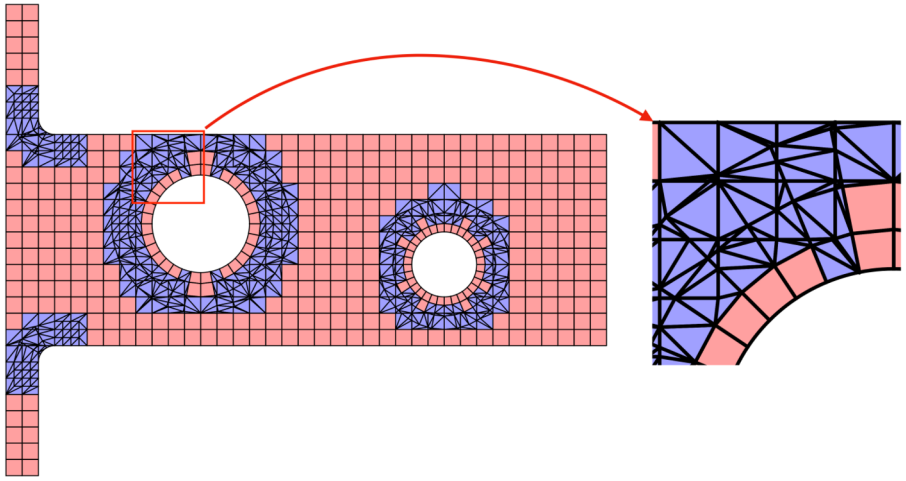

Fig. 4. A mesh overlay and the triangulation.

Table 1
Algorithm to compute the stiffness matrix and load vector of overlapping meshes.

Algorithm MOFEM (2D linear elasticity)

1. **Input:** Material properties, domain Ω, boundary conditions
2. Decompose Ω into m subdomains Ω_i ($i = 1, \ldots, m$).
3. Discretize each Ω_i into mesh $\mathcal{T}_i$.
4. Compute the mesh overlay to obtain a list of triangles (T), a list of non-overlapping elements (Q), a list of vertices (V), and a list of edges (E).
5. Initialize all nodal values of P_i ($i = 1, \ldots, m$) to 1.
6. For each edge in E:
   - If the edge is on (the closure of) some interior boundary Γ_i^* :
     - For each end point of the edge: If the end point is a node in mesh $\mathcal{T}_i$, set the corresponding nodal value of P_i to 0.
7. For each vertex in V:
   - Compute the values of weight functions w_i using Eq. (1).
   - Store these values in an m-dimensional array.
8. For each element in Q:
   - As in traditional finite element analysis, compute the element stiffness matrix.
9. For each triangle in T:
   - For each pair of incident elements:
     - Interpolate corresponding weight functions using their values on vertices.
     - Evaluate strain matrices using Eq. (5) and numerically integrate the sub-matrix in Eq. (7) over the triangle.
10. Assemble the global stiffness matrix.
11. Obtain the force term using Eq. (8).
12. Impose displacement constraints and solve the linear system.

Using Céa's lemma, the solution error is bounded by the interpolation error. Let us consider the interpolation of one displacement component. Let u be the exact solution with $\|u\|_{\max_i(k_i+1)} < \infty$, where k_i is the order of elements in mesh $\mathcal{T}_i$, and $\|\cdot\|_{\max_i(k_i+1)}$ is the $H^{\max_i(k_i+1)}$ norm over domain Ω. Assume there are m meshes. On mesh $\mathcal{T}_i$, it is reasonable to assume due to classic interpolation theory that there exists a local interpolation u_i^* satisfying $|u_i^* - u|_1^{(i)} \le C_i h_i^{k_i}$ and $\|u_i^* - u\|_0^{(i)} \le D_i h_i^{k_i+1}$, where $|\cdot|_1^{(i)}$ is the H^1 semi-norm over Ω_i, $\|\cdot\|_0^{(i)}$ is the L^2 norm over Ω_i, h_i is the maximum size of elements in $\mathcal{T}_i$, and C_i, D_i are constants independent of h_i. Denoting by h the minimum dimension of the overlapped regions $\Omega_j \cap (\cup_{i \neq j} \Omega_i)$ ($j = 1, \ldots, m$) (h can be interpreted as the shortest distance between the interior boundary of Ω_j and the interior boundary of $\cup_{i \neq j} \Omega_i$ for all j), the global interpolation $u^* = \sum_i w_i u_i^*$ satisfies

$$|u^* - u|_1^2 \le 2m \sum_i C_i^2 h_i^{2k_i} + 4m \sum_i D_i^2 d^2 \frac{h_i^2}{(\min\{h_i, h\})^2} h_i^{2k_i} \tag{11}$$

under the assumption $|\frac{\partial w_i}{\partial x}|, \ |\frac{\partial w_i}{\partial y}| \le \frac{d}{\min\{h_i, h\}}$ for some constant d, where $|\bullet|_1$ is the H^1 semi-norm over Ω. The assumption is reasonable because $w_i = 0$ on the interior boundary of Ω_i, $w_i = 1$ on the interior boundary of $\cup_{j \neq i} \Omega_j$, and we interpolate w_i by a piecewise linear function. To prove Inequality (11), we use that $u = \sum_i w_i u$ and the Cauchy-Schwarz inequality. This inequality implies that the global convergence rate is dominated by the lowest order of elements in the overlapping meshes.

Inequality (11) corresponds to our intuition except for the effect of the denominator $\min\{h_i, h\}$ in the inequality. We would expect that if all local interpolations have small errors, the global error should be correspondingly small. Yet, the denominator $\min\{h_i, h\}$ in this inequality tells that as the size h of overlapping tends to zero the error bound increases, unless $h \ge \gamma h_i \ \forall\, i$ with γ a reasonable positive constant. Also, since the above error bound is not tight, convergence may still occur and in numerical experiments we see that the solution obtained corresponds to that of adjoining meshes when h goes to zero with h_i staying finite. A numerical example demonstrating this phenomenon is given in Section 3.2.

While of some value, the error bound in the Inequality (11) is not all encompassing. In addition to the limitation pointed out above, we may want to use a mesh overlapping a base mesh as an interpolation enrichment. The error given by the overlapping meshes in Inequality (11) should be smaller, as also seen in several numerical examples in Section 3. An improvement in the error bound would be valuable.

2.6. Implementation

For an efficient implementation we decompose the analysis domain into an interior subdomain and several boundary subdomains, like proposed in the AMORE scheme. Unless otherwise stated, regular 4-node elements with incompatible modes are used in the interior subdomain (except when the elements are overlapping, the incompatible modes are not used), and higher order elements (9-node finite elements) are used for the boundary subdomains so as to resolve the boundary curvature and obtain accurate local solutions for stress concentrations. An example mesh can be seen in Fig. 3. The solutions to this problem are given in Section 3.3.

We consider a cantilever plate with two holes. Fillets are used to avoid stress singularities. A 4-node element mesh, obtained in the first steps of AMORE [14,15], is spanned over most of the domain (the blue elements), and 9-node element meshes are established near curved boundaries (the red elements). To establish weight functions as well as to numerically integrate the stiffness matrix, the mesh overlay structures need be computed. Here, a mesh overlay is a planar subdivision induced by several overlapping meshes. Since meshes may overlap in any geometric form, their induced planar subdivision is composed of general polygons. The algorithm is designed to output a list of polygons in the overlapped regions and a list of elements that are not overlapping with others. For each polygon, there are pointers to its incident

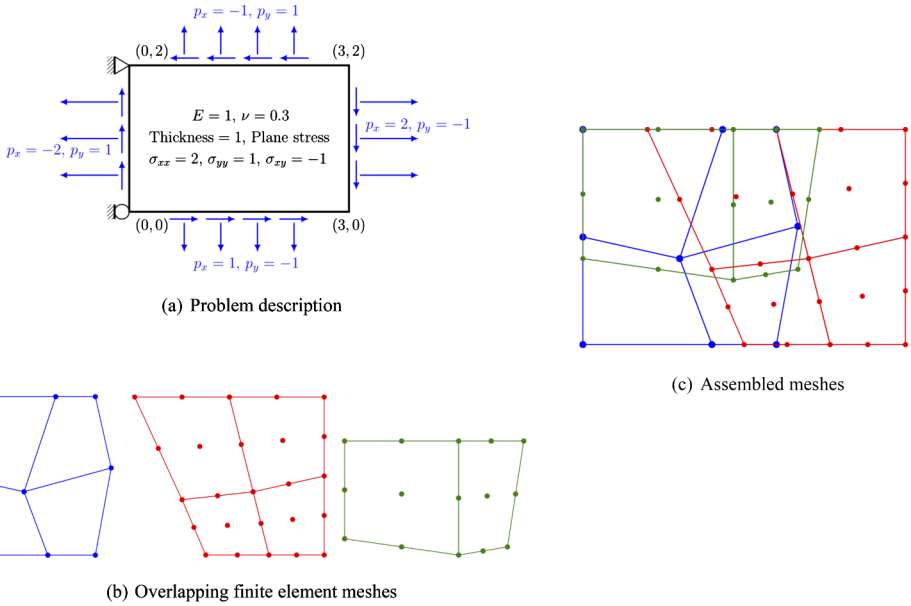

Fig. 5. A patch test problem and overlapping meshes. (a) Problem description, (b) Overlapping finite element meshes, (c) Assembled meshes.

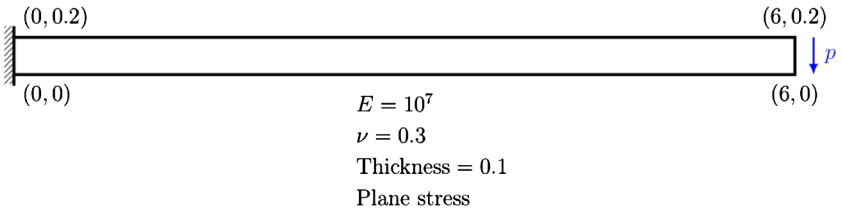

Fig. 6. The thin beam problem, total applied force = 1.

elements, i.e. of which elements the polygon is a part. Each polygon is further triangulated so we can integrate Eq. (7) using existing quadrature schemes [24,25]. A mesh overlay corresponding to the input meshes in Fig. 3 is shown in Fig. 4.

In Fig. 4, the red cells represent elements that do not overlap with any other element. It can be seen that $w_1 = 1$ or $w_2 = 1$ hold on the red region. As a result, these non-overlapping elements are treated as in traditional finite element analysis. The blue region represents the overlapped regions and coupling regions. For numerical integration, the blue region is triangulated. Due to the mutual independence of meshes, the overlapped region will not generally be of regular shape. Some of these triangles may be severely distorted, but this does not matter since the triangles are merely used for numerical integration. They are not triangular finite elements.

Let n be the total numbers of faces (polygons), vertices, and edges in the mesh overlay. The computational time for calculating the mesh overlay and triangulation is $O(n \log n)$ using the well-established plane sweep algorithm and a simple triangulation algorithm. A detailed introduction to the algorithms can be found in references [22,23].

A summary of the complete algorithm used is given in Table 1.

As for many traditional elements, we require the numerical integration to be exact when each of the overlapping meshes is regular [1,26]. For example, to integrate the coupling of two bilinear elements, the two strain matrices are both of order 2, and the integrand in Eq. (7) is of order 4, which requires 6 quadrature points. To integrate the coupling of two 9-node finite elements, since the two strain matrices are both of order 4, the exact numerical integration requires 16 quadrature points.

In the plane sweep algorithm (see references [22,23] for details), a horizontal line (sweep line) moves downwards over the meshes to find all intersections and calculate the mesh overlay structure. We have found that implementing the plane sweep algorithm requires attention on special cases such as overlapping edges and horizontal edges. For this reason, some other algorithms [28–30] for calculating the mesh overlay structure may be more suitable in engineering applications.

3. Numerical examples

The method of overlapping finite elements and meshes has great potential in many fields of finite element analysis. Here we illustrate the use in some example solutions. For comparisons, all traditional finite element solutions are computed and plotted using ADINA.

3.1. Patch tests

The patch tests are used merely for validating the code. As we have already shown in preceding sections, the proposed interpolation technique passes the patch test. As an example, a problem description and overlapping meshes can be seen in Fig. 5.

The rectangular domain is discretized using three independent meshes, as indicated in the figure by different colors. The blue mesh consists of only 4-node elements and 9-node elements are used in the other two meshes.

Since all meshes are distorted, the proposed integration procedure is not exact but the maximum error in the computed stresses is smaller than 0.03%.

3.2. Thin beam problems: Use of overlapping meshes

The physical model problem is depicted in Fig. 6. The reference solution for the tip deflection at the free end is 0.1081, given by Timoshenko beam theory [31]. The numerical solution to the tip deflection obtained using six equal regular 4-node compatible finite elements is 0.0101, which is very inaccurate due to shear locking. On the other

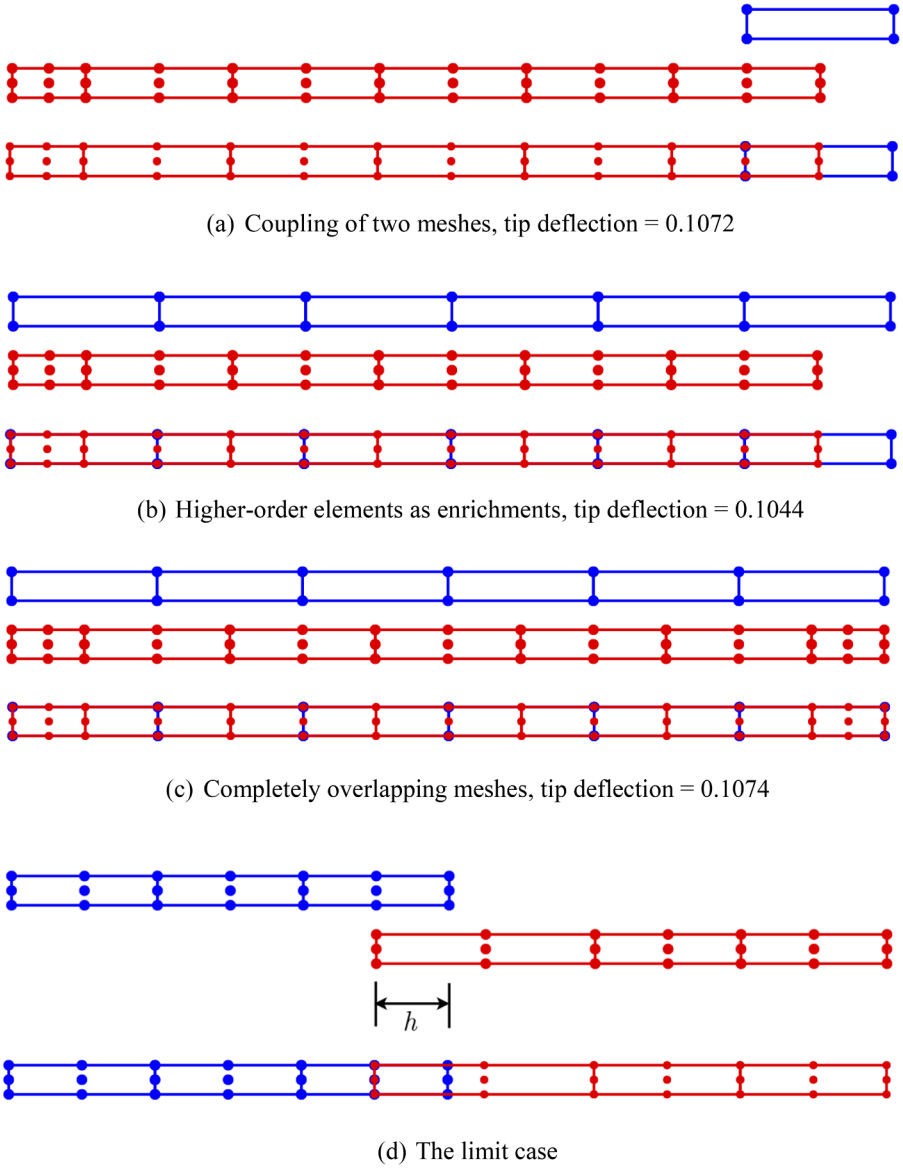

(a) Coupling of two meshes, tip deflection = 0.1072

(b) Higher-order elements as enrichments, tip deflection = 0.1044

(c) Completely overlapping meshes, tip deflection = 0.1074

(d) The limit case

Fig. 7. Different overlapping meshes for the thin beam problem. (a) Coupling of two meshes, tip deflection = 0.1072, (b) Higher-order elements as enrichments, tip deflection = 0.1044, (c) Completely overlapping meshes, tip deflection = 0.1074, (d) The limit case.

Table 2
Tip deflections at different overlapping sizes h.

h	0.5	0.1	0.01	0.001	0.0001
Tip deflection	0.106946	0.107049	0.107040	0.107035	0.107034

hand, the use of six equal regular 9-node finite elements leads to a tip deflection at 0.1070.

We use this simple analysis case to demonstrate the solutions when different simple meshes are overlapping.

3.2.1. Coupling of meshes used in different regions

An attractive use is to use a high-order finite element mesh for a region with large stress gradients, and a low-order finite element mesh for the remaining region. Just to test this idea, we consider the simple case in Fig. 7(a). The numerical solution in this case is 0.1072.

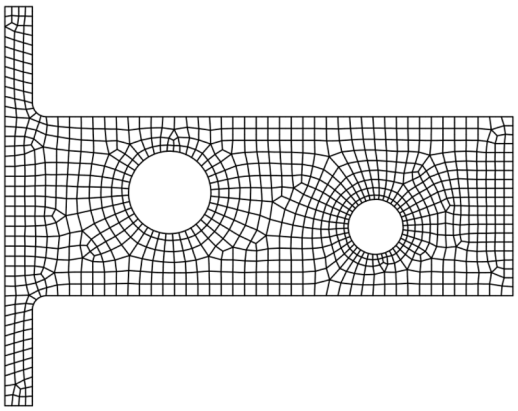

Fig. 8. A traditional free-form 9-node finite element mesh giving the FE solution.

3.2.2. Higher-order elements as enrichments

We may also use a higher-order mesh overlaying a lower-order base mesh to obtain better local solutions. In Fig. 7(b) we consider a simple case. The resulting numerical solution is 0.1044, which is much better than the locking solution given when using only 4-node finite elements. However, this solution is slightly worse than when just using six 9-node

Table 3
Numerical solutions for the plate with two holes.

	AMORE-FE	AMORE-ICM	FE solution	Reference
Energy	1.9891	1.9922	1.9870	1.9962
u_{max}	0.11313E-3	0.11332E-3	0.11325E-3	0.11352E-3
u_{min}	−0.10349E-3	−0.10364E-3	−0.10353E-3	−0.10377E-3
τ_{xxmax}	18.190E3	18.205E3	18.017E3	19.135E3
τ_{xxmin}	−18.284E3	−18.295E3	−18.013E3	−19.181E3
$\bar{\tau}_{max}$	19.124E3	19.135E3	18.935E3	19.673E3
Number of dofs	3,070	3,070	7,724	>98,000
NNZ*	120,769	120,769	120,690	>1,602,000

* NNZ: Number of non-zero sparse matrix entries.

elements because the coupled interpolation fails to reproduce an arbitrary quadratic polynomial. In addition, of course, this solution requires considerably more computations and hence is usually not attractive. However, the technique may be promising for adaptation.

3.2.3. Completely overlapping meshes

In Fig. 7(c) the second mesh completely covers the first mesh. The corresponding numerical solution is 0.1074. For the completely overlapping meshes we have a linear combination of two traditional interpolations with constant coefficients. Therefore, the coupling interpolation is in this case better than using either the 4-node element interpolation or the 9-node element interpolation.

However, we should recall the theoretical condition for the (coupling) interpolation to be solvable. If one mesh interpolation is in some way contained in the other mesh interpolation – which is here the case – the condition is violated. Nevertheless, in this case the solver still provided the solution due to round-off.

3.2.4. The limit case

We mention in Section 2.5 that if the overlapped region tends to a curve, the numerical solution may converge to the solution given by the corresponding non-matching meshes. Here we give the solutions of an example.

Fig. 7(d) shows two 9-node finite element meshes overlapping and the overlapped region has a characteristic "size" h. Numerical solutions of the tip deflection are listed in Table 2 as a function of h.

The table shows that as h tends to zero, the tip deflection converges to 0.107034, which is exactly the solution obtained with six 9-node finite elements in a regular conforming mesh.

3.3. AMORE in the analysis of a plate with two holes

The problem shown in Fig. 3 has been introduced in Section 2.6.

To demonstrate the performance of the proposed scheme, we compare the numerical solutions with those of a traditional 9-node finite element mesh in ADINA. The traditional mesh is shown in Fig. 8, and the solution obtained with this mesh is called "FE solution" in Table 3.

In the AMORE solution, obtained with the meshes given in Fig. 3(b) we use as non-overlapping 4-node elements in a first solution the 4-node traditional element and in a second solution the 4-node element

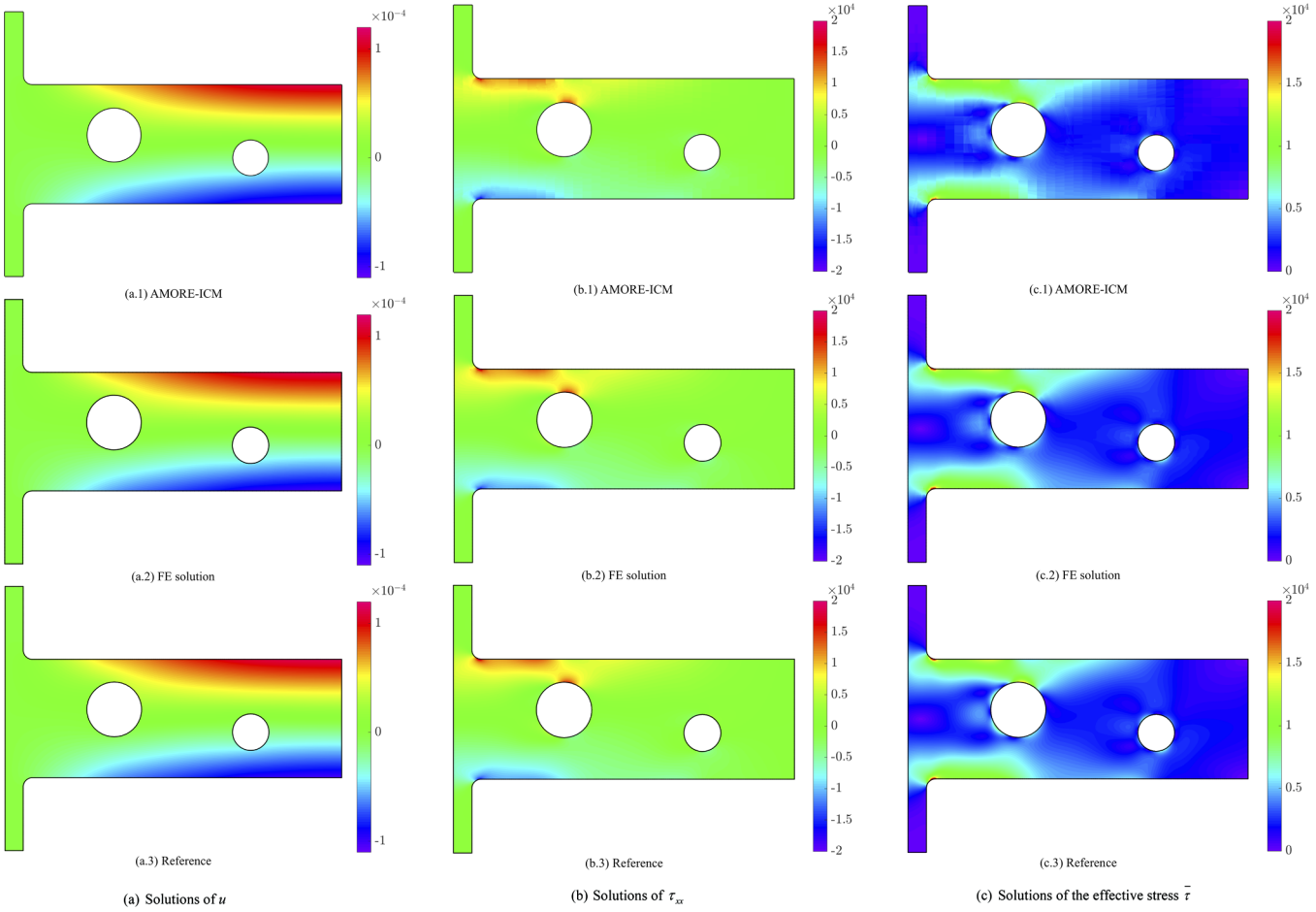

Fig. 9. Numerical solutions for the plate with two holes. (a) Solutions of u (a.1) AMORE-ICM (a.2) FE solution (a.3) Reference, (b) Solutions of τ_{xx} (b.1) AMORE-ICM (b.2) FE solution (b.3) Reference, (c) Solutions of the effective stress $\bar{\tau}$ (c.1) AMORE-ICM (c.2) FE solution (c.3) Reference.

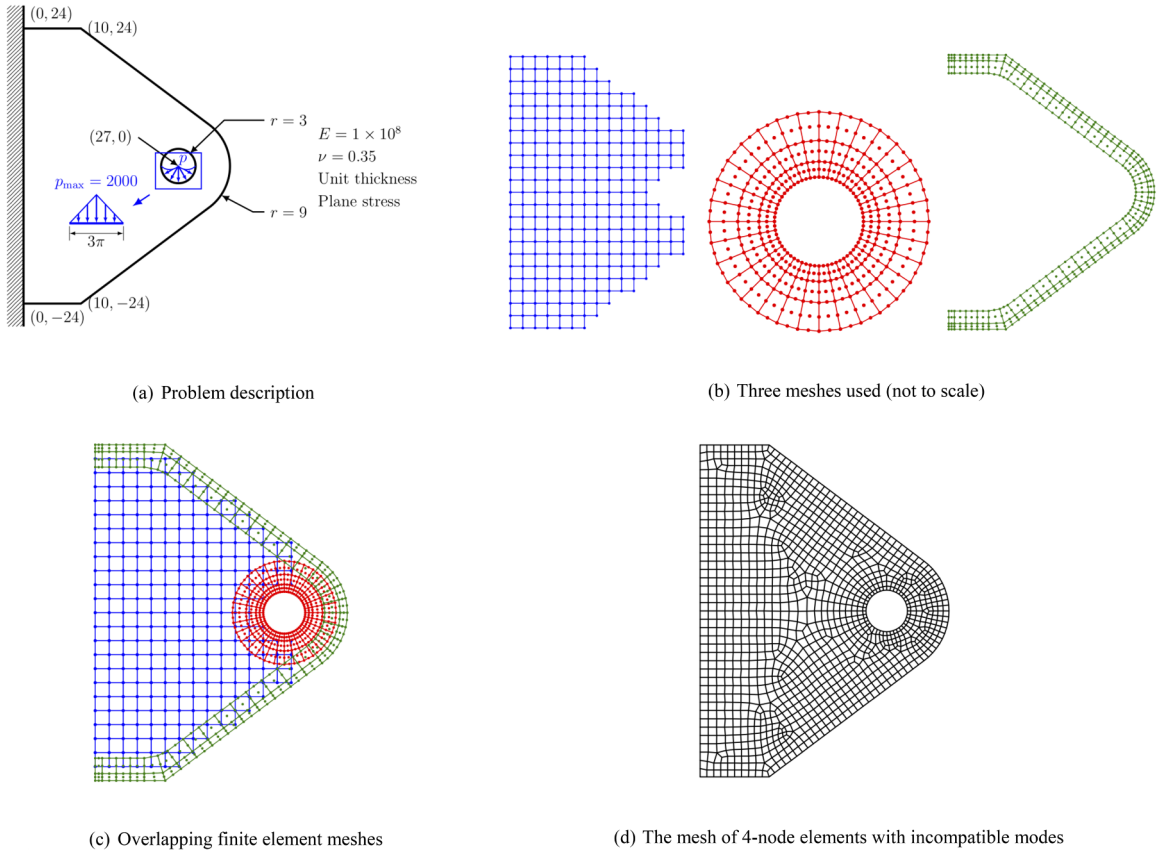

(a) Problem description

(b) Three meshes used (not to scale)

(c) Overlapping finite element meshes

(d) The mesh of 4-node elements with incompatible modes

Fig. 10. A bracket with a hole. (a) Problem description, (b) Three meshes used (not to scale), (c) Overlapping finite element meshes, (d) The mesh of 4-node elements with incompatible modes.

Table 4
Numerical solutions for the bracket with a hole.

	AMORE-ICM	ICM solution	Reference
Energy	1.0617	1.0551	1.0630
$\nu_{\min}$	−0.29732E-3	−0.29597E-3	−0.29777E-3
$\tau_{xy\min}$	−1.4079E3	−1.3531E3	−1.4560E3
$\bar{\tau}_{\max}$	2.5129E3	2.5560E3	2.5732E3
Number of dofs	2,156	2,480	>166,000
NNZ*	94,750	22,516	>2,722,000

* NNZ: Number of non-zero sparse matrix entries.

with incompatible modes [1]. The solutions are named “AMORE-FE” and “AMORE-ICM”, respectively. Some numerical results are listed in Table 3 as well as plotted in Fig. 9. The reference solutions are obtained using ADINA with a very fine mesh of 9-node elements. Note that all stress results using AMORE are plotted without stress smoothing.

Figs. 3 and 4 show that most elements in the overlapping meshes are non-overlapping. The increase in solution effort is due to the overlapping and the coupling regions. The coupling between the meshes leads to a larger bandwidth and increases the number of non-zero entries of the stiffness matrix (NNZ). The relatively small overlapped regions in this problem render the use of the overlapping meshes quite effective. Note that since we use 9-node elements near the boundaries to resolve the curvature and stress concentrations, the resulting stress solutions are accurate.

3.4. AMORE in the analysis of bracket problems

In general, the overlapping and number of overlapping meshes best used depends on the problem to be solved. Although using two meshes that overlap at a location is usually sufficient, the use of more meshes that overlap at a specific location can make the meshing process easier. In this section, instead of using only two meshes that overlap at a specific point, we present the solutions to bracket problems using more overlapping finite element meshes. We will also show why the number of overlapping meshes should not be too large.

3.4.1. A bracket with a hole

This problem is described in Fig. 10, where also the overlapping meshes are given. The bracket is fixed on the left boundary and loaded on its hole. We use three overlapping meshes to discretize the analysis domain. For the interior domain (the blue mesh) 4-node incompatible modes (ICM) elements are used, and 9-node finite elements are used near the boundary (the red and green meshes).

A mesh of 4-node elements with incompatible modes automatically generated in ADINA is used for comparison, as shown in Fig. 10(d). We refer to this solution as the “ICM solution”. The reference solution has been obtained using a very fine mesh of 9-node elements with ADINA.

Numerical results to this problem are given in Table 4 and Fig. 11. All stresses are not smoothed. The ICM solution shows a reasonable accuracy and the AMORE-ICM discretization gives accurate stress predictions. Note that in ADINA, the stress field is extrapolated from the solutions at the Gauss points, while in the implementation used here, the stresses have been calculated at the points of interest directly by the displacement solution.

In this example, we also notice that the number of non-zero sparse matrix entries (NNZ) is much larger using AMORE than in the traditional finite element analysis, although the numbers of dofs are close. However, the corresponding increase in solution time is reasonable as we are able to save much human effort for meshing.

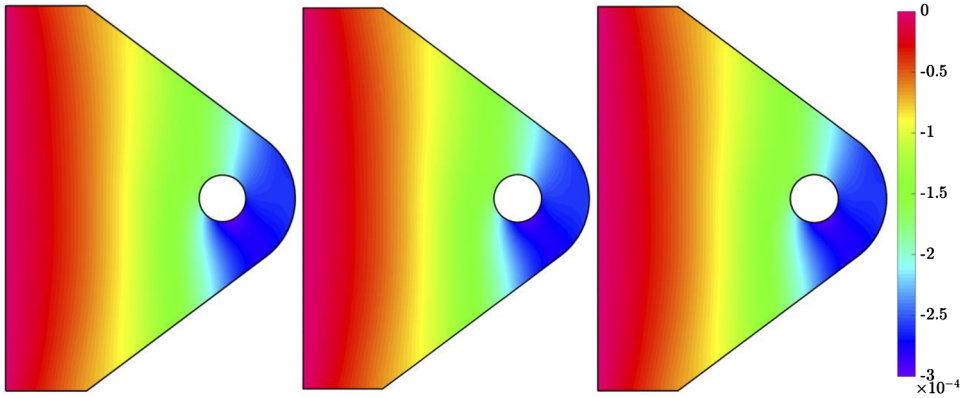

(a) Solutions of v (Left: AMORE-ICM; Middle: ICM solution; Right: Reference)

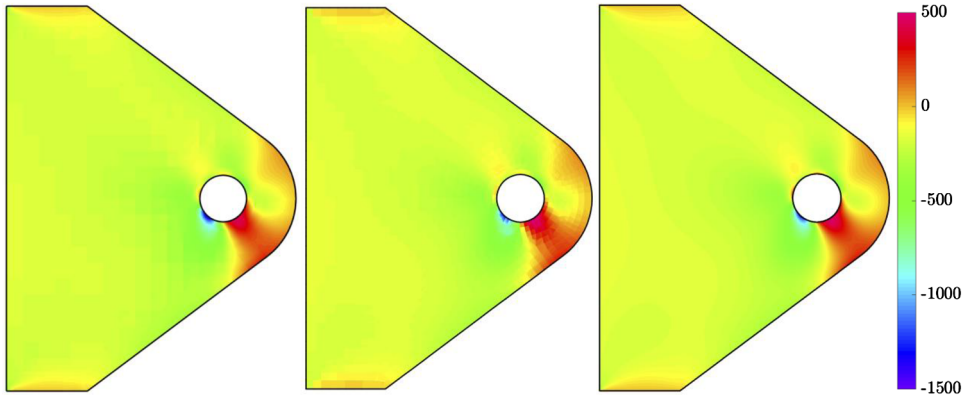

(b) Solutions of τ_{xy}

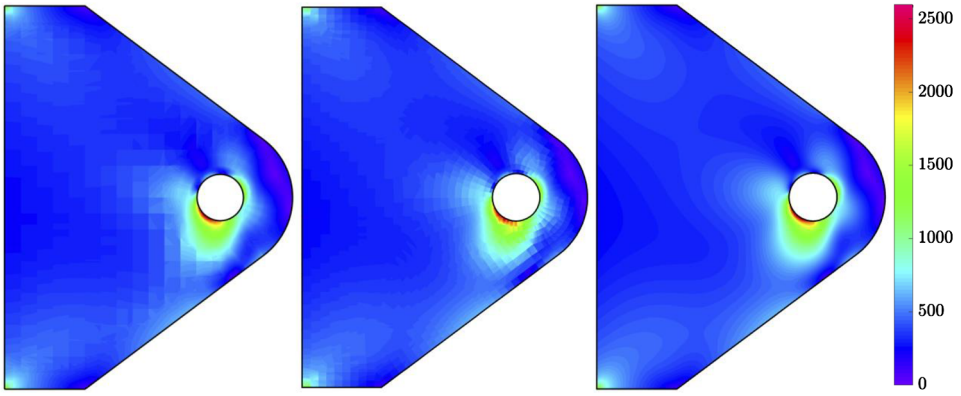

(c) Solutions of $\bar{\tau}$

Fig. 11. Numerical solutions for the bracket with a hole. (a) Solutions of v (Left: AMORE-ICM; Middle: ICM solution; Right: Reference), (b) Solutions of τ_{xy}, (c) Solutions of $\bar{\tau}$.

3.4.2. A bracket with an inclusion

We also want to illustrate the potential of the scheme to simplify the meshing of regions of different materials and their interfaces. In traditional finite element analysis, meshes of regions of different materials typically match on the interfaces, but a gluing (like available in ADINA), or other scheme, could also be used. Complexity of the interface may bring additional difficulties to the meshing process.

Consider a bracket geometrically similar to the bracket in Section 3.4.1, but having an inclusion. At the center of the inclusion, a concentrated force is applied. The problem description, the overlapping

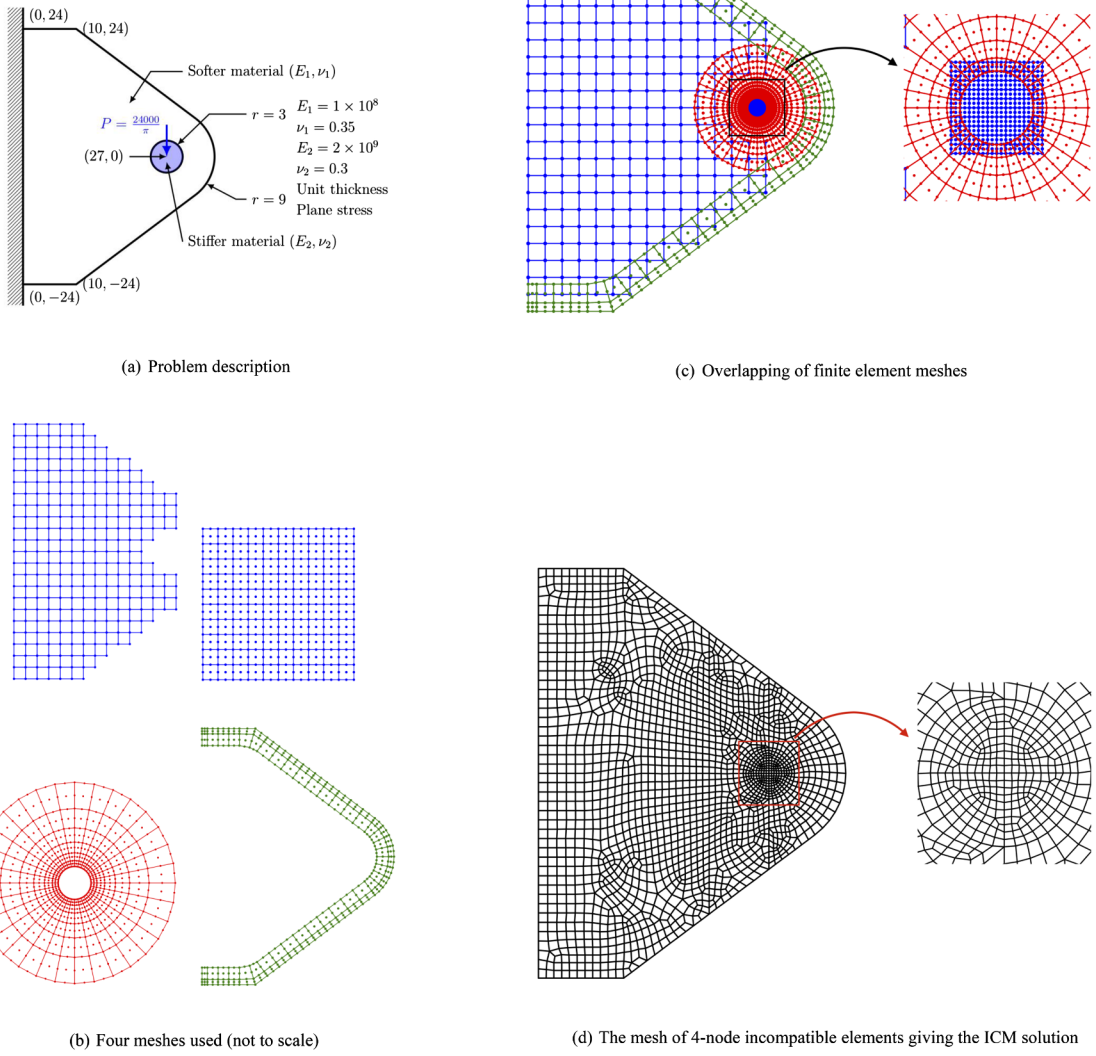

Fig. 12. A bracket with a stiff inclusion. (a) Problem description, (b) Four meshes used (not to scale), (c) Overlapping of finite element meshes, (d) The mesh of 4-node incompatible elements giving the ICM solution.

Table 5
Numerical solutions for the bracket with a stiff inclusion.

	AMORE-ICM	ICM solution	Reference
Energy	0.82215	0.81867	0.83044
$v_{\min}$	−2.4056E-4	−2.4052E-4	−2.4069E-4
$\bar{\tau}_{\max}$	5.0424E4	1.5969E4	23.921E4 (+∞)
Number of dofs	3,806	3,934	>331,000
NNZ*	210,690	36,577	>5,443,000

* NNZ: Number of non-zero sparse matrix entries.

meshes and a traditional mesh used for comparison are presented in Fig. 12. Using the proposed AMORE meshing scheme, the process of meshing the interface is relatively simple, as shown in Fig. 12.

Some results of the numerical solution are listed in Table 5 and plotted in Fig. 13. The reference solution has been obtained with a very fine mesh of 9-node elements.

The solutions share some similarities with those presented in Section 3.4.1 but also show some new features since the Young's modulus of the inclusion is twenty times that of the bracket. We show in this case the dominant displacement component v and the effective stress $\bar{\tau}$. In the overlapping meshes, we use a very fine 9-node finite element mesh for the interior of the inclusion. It is not very judicious to compare predicted stresses at stress singularities, but if we do, we see in Fig. 13 that the proposed procedure gives a more reasonable local stress solution (using 9-node elements for the inclusion) than the fine traditional mesh of 4-node incompatible modes elements. If the local solution is not important, the mesh we used to represent the inclusion could be coarser to save computational effort. Note that in this case the value of NNZ is much larger when using AMORE, for the reasons given in Section 3.4.1.

4. Concluding remarks

We proposed a method of overlapping finite element meshes for the AMORE scheme in which a global compatible interpolation is obtained, local refinement can be achieved efficiently, the resulting equilibrium equations can be solved with direct sparse solvers, and the meshing process can be highly automated with a reasonable computational expense.

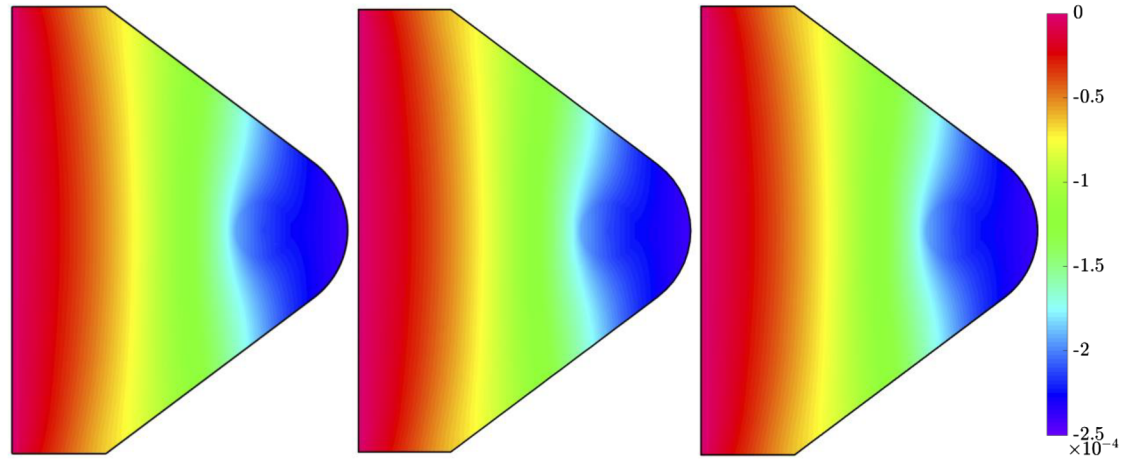

(a) Solutions of v (Left: AMORE-ICM; Middle: ICM solution; Right: Reference)

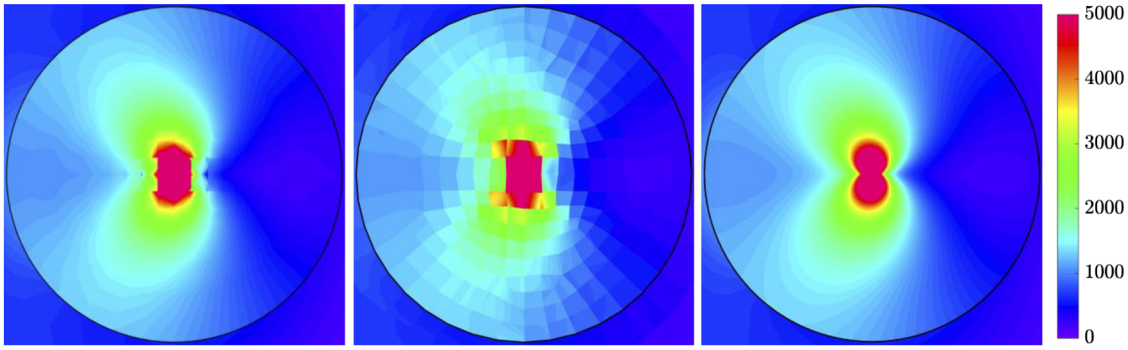

(b) Solutions of $\bar{\tau}$ inside the inclusion

Fig. 13. Numerical solutions for the bracket with a stiff inclusion. (a) Solutions of v (Left: AMORE-ICM; Middle: ICM solution; Right: Reference), (b) Solutions of $\bar{\tau}$ inside the inclusion.

Using AMORE, the analysis domain is decomposed into several subdomains. If each subdomain is of regular shape, it can be meshed effectively with conventional finite elements, and ideally with undistorted elements because the elements then perform best. The meshes overlap and cover the whole analysis domain. On each mesh, a continuous weight function is established using low-order finite element interpolations. These weight functions form a partition of unity over the analysis domain. The weighted average of local interpolations is the desired global compatible interpolation.

We analyzed the solvability and gave an error bound to give theoretical evidence for the proposed scheme to work in the solution of general problems. The numerical examples illustrated the use of the scheme. The procedure can be conveniently applied to many practical engineering problems and automated to significantly simplify the meshing process. However, many topics of research should be pursued to increase the effectiveness and the applicability of the scheme.

Since meshes can overlap in any geometric form, a good implementation requires efficient algorithms and data structures for calculating the overlay of several finite element meshes. The plane sweep algorithm was used in this paper, but the use of more suitable geometric algorithms should be explored [28–30].

Compared with traditional finite element analysis, the proposed scheme may increase the number of non-zero entries in the stiffness matrix, which indicates an increase in the solution effort. This increase in solution effort may be small, and indeed less computations may even be used with overlapping meshes for a given accuracy of solution if the regions of overlapping are small and only two meshes overlap at a location. Special sparse solvers may increase the effectiveness of solving the equations.

A better a-priori error estimate is needed to understand the error introduced by the coupling interpolation. The error estimate should be able to accurately predict the enriching effect of higher-order meshes as well as giving the error in case the overlapped region decreases in size. An a-posterior error bound would be equally useful.

A research effort is needed to improve the scheme used in the paper to numerically integrate the element matrices, and also to improve the stress predictions obtained from the overlapping elements. Considering traditional finite elements, frequently specific locations give better stress predictions than other points [1]. There may be similar situations in the method of overlapping finite element meshes.

The procedure should be extended to the solution of three-dimensional problems. The ideas used in this paper can, in principle, be used but the complexity in three dimensions requires additional research.

With the large inherent potential in the use of AMORE, the scheme

should also be extended for use in the nonlinear analysis of solids, including contact, and for the solution of fluid mechanics and multi-physics problems.

Declaration of Competing Interest

None.

References

[1] Bathe KJ. Finite element procedures. Prentice hall; 1996. 2nd ed. Watertown: K.J. Bathe; 2014 and Beijing: Higher Education Press; 2016.
[2] Chesshire G, Henshaw WD. Composite overlapping meshes for the solution of partial differential equations. J Comput Phys 1990;90(1):1–64.
[3] Steger JL, Benek JA. On the use of composite grid schemes in computational aerodynamics. Comput Methods Appl Mech Eng 1987;64(1–3):301–20.
[4] Benek JA, Buning PG, Steger JL. A 3-D Chimera grid embedding technique. In: 7th Computational physics conference, Cincinnati, USA, 1985.
[5] Dolean V, Jolivet P, Nataf F. An introduction to domain decomposition methods: Algorithms, theory and parallel implementation. SIAM; 2015.
[6] Strouboulis T, Copps K, Babuška I. The generalized element method. Comput Methods Appl Mech Eng 2001;190(32–33):4081–193.
[7] Strouboulis T, Babuška I, Copps K. The design and analysis of the generalized finite element method. Comput Methods Appl Mech Eng 2000;181(1–3):43–69.
[8] Duarte CA, Babuška I, Oden JT. Generalized finite element methods for three-dimensional structural mechanics problems. Comput Struct 2000;77(2):215–32.
[9] Hansbo A, Hansbo P, Larson M. A finite element method on composite grids based on Nitsche's method. ESAIM: Math Model Numer Anal 2003;37(3):495–514.
[10] Massing A, Larson MG, Logg A. Efficient implementation of finite element methods on nonmatching and overlapping meshes in 3D. SIAM: J Sci Comput 2013;35(1):23–47.
[11] Glowinski R, Pan T-W, Hesla TI, Joseph DD. A distributed Lagrange multiplier/fictitious domain method for particulate flows. Int J Multiph Flow 1999;25(5):755–94.
[12] Glowinski R, Pan T-W, Periaux J. A fictitious domain method for Dirichlet problem and applications. Comput Methods Appl Mech Eng 1994;111(3–4):283–303.
[13] Bathe KJ, Khoshgoftaar MR. Finite element free surface seepage analysis without mesh iteration. Int J Num Anal Methods Géoméch 1979;3(1):13–22.
[14] Bathe K.J. The finite element method with “overlapping finite elements”. In: Zingoni A, editor. Proceedings sixth international conference on structural engineering, mechanics and computation – SEMC 2016, Cape Town, South Africa, 2016.
[15] Bathe KJ. The AMORE paradigm for finite element analysis. Adv Eng Softw 2019;130:1–13.
[16] Bathe KJ, Zhang L. The finite element method with overlapping elements – A new paradigm for CAD driven simulations. Comput Struct 2017;182:526–39.
[17] Zhang L, Bathe KJ. Overlapping finite elements for a new paradigm of solution. Comput Struct 2017;187:64–76.
[18] Zhang L, Kim KT, Bathe KJ. The new paradigm of finite element solutions with overlapping elements in CAD – Computational efficiency of the procedure. Comput Struct 2018;199:1–17.
[19] Huang J, Bathe KJ. Quadrilateral overlapping elements and their use in the AMORE paradigm. Comput Struct 2019;222:25–35.
[20] Kim KT, Zhang L, Bathe KJ. Transient Implicit Wave Propagation Dynamics with Overlapping Finite Elements. Comput Struct 2018;199:18–33.
[21] Kim J, Bathe KJ. The finite element method enriched by interpolation covers. Comput Struct 2013;116:35–49.
[22] de Berg M, Cheong O, van Kreveld M, Overmars M. Computational geometry: Algorithms and applications. 3rd ed. Berlin Heidelberg: Springer-Verlag; 2008.
[23] Bentley JL, Ottmann TA. Algorithms for reporting and counting geometric intersections. IEEE Trans Comput 1979;C-28(9):643–7.
[24] Cowper GR. Gaussian quadrature formulas for triangles. Int J Numer Methods Eng 1973;7(3):405–8.
[25] Dunavant DA. High degree efficient symmetrical Gaussian quadrature rules for the triangle. Int J Num Methods Eng 1985;21(6):1129–48.
[26] Ciarlet PG. The finite element method for elliptic problems. SIAM; 2002.
[27] Chapelle D, Bathe K.J. The finite element analysis of shells – Fundamentals. 2nd ed. Springer; 2011.
[28] van Oosterom P. An R-tree based map-overlay algorithm. In: Proceedings EGIS/MARI’94, Paris, France, 1994.
[29] Finke U, Hinrichs KH. Overlaying simply connected planar subdivisions in linear time. In: Proceedings of the eleventh annual symposium on computational geometry, Vancouver, Canada, 1995.
[30] Franklin WR, Narayanaswaml C, Kankanhalll M, Sun D, Zhou MC, Wu PY. Uniform grids: A technique for intersection detection on serial and parallel machines. In: Proceedings of Auto-Carto 9, Maryland, USA, 1989.
[31] Bucalem ML, Bathe K.J. The mechanics of solids and structures – Hierarchical modeling and the finite element solution. Springer; 2011.